NACA RM L54K24a

NACA

RESEARCH MEMORANDUM

FLIGHT INVESTIGATION AND ANALYSIS OF THE WING DEFORMATIONS OF A SWEPT-WING BOMBER DURING PUSH-PULL MANEUVERS

By Alton P. Mayo and John F. Ward

Langley Aeronautical Laboratory
Langley Field, Va.

NATIONAL ADVISORY COMMITTEE
FOR AERONAUTICS

WASHINGTON

April 14, 1955

NATIONAL ADVISORY COMMITTEE FOR AERONAUTICS

RESEARCH MEMORANDUM

FLIGHT INVESTIGATION AND ANALYSIS OF THE WING DEFORMATIONS OF A SWEPT-WING BOMBER DURING PUSH-PULL MANEUVERS

By Alton P. Mayo and John F. Ward

SUMMARY

The results of deflection measurements made at 12 stations on the wing of a swept-wing jet bomber (Boeing B-47A) during 18 push-pull maneuvers are presented in the form of coefficients expressing the deflections due to the zero-lift loads, the additional-lift loads, the pitching-angular-acceleration loads, and the pitching-angular-velocity loads on the airplane. The procedures used to obtain the coefficients are presented along with comparisons of the experimental deflection and twists with those obtained from theoretical calculations.

INTRODUCTION

In the calculation of the loads on a flexible airplane, it is necessary to have accurate methods of determining the amount of structural deflection. Especially is this true in the calculation of the loadings on swept wings where the local angle of attack may be greatly affected by the deflection of the wing. In order to obtain knowledge of the aeroelastic behavior of an actual swept wing in flight and to obtain experimental data by which to check theoretical methods, one phase of a flight research program on the Boeing B-47A, conducted by the National Advisory Committee for Aeronautics, has included the installation of an optigraph system to record the in-flight deflections of the wing.

This paper will be concerned with the wing deflection measurements made during push-pull maneuvers, and the reduction of the flight data to coefficients expressing the wing deflections due to the zero-lift load, the additional-lift and inertia load, and the pitching-acceleration and pitching-velocity loads on the airplane. Comparisons are made between the experimental results and theoretical calculations.

SYMBOLS

Z	total optigraph target deflection measured from wing drooped position (ground zero), positive upward, in.
Z_0	target deflection due to the wing airloads when the summation of the aerodynamic loads on the airplane is zero, positive upward, in.
$Z_{0_{wf}}$	target deflection due to the wing airloads when the summation of the airload on the wing and fuselage is zero, positive upward, in.
Z_n	target deflection per unit airplane normal load factor, positive upward, in./n
$Z_{n_{wf}}$	target deflection due to the additional-lift load on the wing and fuselage, positive upward, in./lb
Z_i	target deflection due to wing inertia under an airplane normal load factor of 1, positive upward, in./n
$Z_{\ddot{\theta}}$	target deflection per unit airplane pitching acceleration, positive upward, in./radians/sec^2
$Z_{\ddot{\theta}_i}$	target deflection due to inertia of the wing with unit pitching acceleration, positive upward, in./radians/sec^2
$Z_{\dot{\theta}}$	target deflection per unit airplane pitching velocity, positive upward, in./radians/sec
$Z_{\dot{\theta}_w}$	target deflection due to unit pitching velocity of the wing alone, in./radians/sec
b'	wing span less fuselage width, in.
I_y	airplane pitching moment of inertia, lb-in.^{2}
L_T	tail load, positive upward, lb
L_{T_0}	tail load when the airplane normal load factor equals zero, positive upward, lb
l_T	distance between center of gravity of airplane and $\bar{c}/4$ of tail, in.

n	airplane normal load factor, positive when inertia loads are downward ($n = 1$ in level flight)
q	dynamic pressure, lb/sq in.
W	airplane weight, lb
X	streamwise distance from intersection of front spar center line and airplane center line, positive aft, in.
Y	lateral distance from airplane center line, positive left, in.
Y'	lateral distance from airplane center line less one-half the fuselage width, positive left, in.
$\dot{\theta}$	airplane pitching angular velocity, positive for airplane nose pitching up, radians/sec
$\ddot{\theta}$	airplane pitching angular acceleration, positive for increasing positive pitching velocity, radians/sec^2
S_Z	standard error of estimate, in.
S_{Z_0}	standard error of the Z_0 coefficient, in.
S_{Z_n}	standard error of the Z_n coefficient, in.
$S_{Z_{\ddot{\theta}}}$	standard error of the $Z_{\ddot{\theta}}$ coefficient, in.
$S_{Z_{\dot{\theta}}}$	standard error of the $Z_{\dot{\theta}}$ coefficient, in.

AIRPLANE AND TESTS

The airplane used in the test was a Boeing B-47A airplane. (See figs. 1 and 2.) The changes in the test airplane configuration from the standard airplane were the installation of (1) an airspeed measuring boom and fairing on the nose and (2) an external canopy, housing the deflection-recording instruments, mounted atop the fuselage approximately at the intersection of the airplane center line and the wing 38-percent-chord line.

The flight-test data used in this paper pertain to push-pull maneuvers flown during the B-47 flight research program conducted at the NACA High-Speed Flight Station at Edwards, Calif.

The push-pull maneuvers were made at altitudes of 25,000, 30,000, and 35,000 feet with Mach numbers ranging from 0.51 to 0.80. The maneuvers were flown with aircraft gross weights of approximately 108,000 and 125,000 pounds, and center-of-gravity positions of 13- and 22-percent mean aerodynamic chord. The normal load factor ranged from 0.3 to 1.5 and pitching accelerations from 0.16 to -0.14 radian per second per second. The specific values of Mach number, altitude, aircraft weight, center-of-gravity position, and dynamic pressure are included in table 1 for each run analyzed in this report.

INSTRUMENTATION AND ACCURACY OF MEASUREMENT

The instrumentation on the airplane which was pertinent to the results presented in this paper consisted of a pitch turnmeter, roll turnmeter, altimeter, airspeed indicator, accelerometer, aileron position recorder, and an optigraph system for recording the wing deflections. The roll turnmeter and aileron position recorder were used only to insure that the data selected were for push-pull maneuvers with little or no roll. The accelerometer was of the single-component type and oriented so as to measure only the normal load factors. The accelerometer was located at 34.25 percent mean aerodynamic chord (x = 241 in.), and the pitch turnmeter was located at 27.19 percent mean aerodynamic chord (x = 230 in.). No corrections were made to the data for the small displacements of the instruments from the airplane center of gravity. All instruments were of the standard NACA photographically recording type with the exception of the optigraph system which was designed by the NACA especially for the B-47A airplane.

The wing optigraph system consisted of eight target lamps on the left wing and four on the right wing and optical recording instruments located atop the fuselage approximately at the intersection of the 38-percent-chord line of the wing and the center line of the fuselage. (See fig. 3.) To facilitate recording the deflections optically in the daylight, high-intensity (rich in infrared) light sources were used in combination with infrared-sensitive recording film. The optigraph system was calibrated through the use of a calibration stick, with 12 lamps on it at 6-inch intervals, held vertically at each target station during the calibration. All in-flight measurements were made with reference to the wing droop position with the airplane on the ground and with the wing outrigger gear clear.

In connection with the optigraph system, a check was made of the errors introduced by possible movements of the optigraph base during conditions of large wing deflections. This check was made to insure that small twists of the wing center section on which the optigraph was mounted would not introduce large apparent deflections or twist at any of the target stations. These tests showed that the optigraph undergoes no appreciable movement with respect to a plane through the wing attachment fittings and that the twist of the optigraph under a 2g wing load could cause a maximum error of 1/2 inch per g at the wing tip and proportionately less error at the other stations. The estimated accuracy of the total deflections from ground zero, calculated from the optigraph film readings, is ±0.4 inch; whereas all incremental in-flight deflections are estimated to be accurate to ±0.2 inch.

The normal load factor and pitching-angular-velocity values used are estimated to be accurate to ±0.01 and ±0.005 radian per second, respectively. The pitching-angular-acceleration values were obtained from measurements of the slopes of the pitching-velocity trace and are estimated to be accurate to ±0.01 radian per second per second. The airplane weights listed in table 1 apply at the time of the maneuver and are estimated to be accurate to ±500 pounds.

RESULTS AND DISCUSSION

Basic Data Reduction

Typical examples of the in-flight measurements plotted in different ways are shown in figures 4, 5, and 6. The time relationship between the deflections and the airplane motions are shown in figure 4, and the variation of the deflections with normal load factor is illustrated in figure 5. Figure 6 shows the deflection of the wing in level flight as obtained from the flight measurements plotted against the span position of the targets.

The procedure by which such in-flight measurements were reduced to deflection coefficients expressing the deflections due to the zero-lift load, additional-lift and inertia load, and pitching-velocity and pitching-acceleration loads on the airplane is as follows: If the fuselage airloads are assumed to vary linearly with the wing additional-lift loads, then the deflection Z of any target on the wing at any instant during a push-pull may be written in terms of the normal load factor, pitching angular acceleration, and pitching angular velocity as

$$Z = Z_0 + Z_{n_{wf}}\left(nW - L_T\right) + Z_{\ddot{\theta}_i}\ddot{\theta} + Z_i n + Z_{\dot{\theta}_w}\dot{\theta} - Z_i \qquad (1)$$

If the tail load is represented by

$$L_T = L_{T_0} + \frac{dL_T}{dn} n + \frac{dL_T}{d\ddot{\theta}} \ddot{\theta} + \frac{dL_T}{d\dot{\theta}} \dot{\theta} \tag{2}$$

the deflection may be expressed by

$$Z = \left(Z_{0_{wf}} - Z_{n_{wf}} L_{T_0}\right) + \left(Z_{n_{wf}} W - Z_{n_{wf}} \frac{dL_T}{dn} + Z_i\right) n + \left(Z_{\ddot{\theta}_i} - Z_{n_{wf}} \frac{dL_T}{d\ddot{\theta}}\right) \ddot{\theta} +$$

$$\left(Z_{\dot{\theta}_{wf}} - Z_{n_{wf}} \frac{dL_T}{d\dot{\theta}}\right) \dot{\theta} - Z_i \tag{3}$$

or more simply by

$$Z = Z_0 + Z_n n + Z_{\ddot{\theta}} \ddot{\theta} + Z_{\dot{\theta}} \dot{\theta} - Z_i \tag{4}$$

During the test, the Mach number, dynamic pressure, weight, and center-of-gravity position were held effectively constant for each run.

Thus, for each target in each run, the deflections may be represented in matrix notation:

$$\{Z\} = \left(Z_0 - Z_i\right)\{1\} + Z_n \{n\} + Z_{\ddot{\theta}} \{\ddot{\theta}\} + Z_{\dot{\theta}} \{\dot{\theta}\} \tag{5}$$

where the columns $\{\ \}$ are corresponding values of Z, n, $\ddot{\theta}$, and $\dot{\theta}$ read from flight records at 0.2-second intervals during the run and the constant Z_i is the deflection of the target due to the dead weight of the wing. The coefficients $Z_0 - Z_i$, Z_n, $Z_{\ddot{\theta}}$, and $Z_{\dot{\theta}}$ for each target were solved for by the method of least squares using approximately 25 data points per run.

When the in-flight deflections Z are plotted against normal load factor, the data assume the distributions shown in figure 5. The solid lines represent the variations of the target deflections with load factor based on the values of $Z_0 - Z_i$ determined for each of the targets by use of least-squares procedures applied to equations of the type of equation (5). The slope of the line is the coefficient Z_n of equation (5)

and the intercept of the line at $n = 0$ is the coefficient $Z_0 - Z_i$. The coefficients $Z_{\ddot{\theta}}$ and $Z_{\dot{\theta}}$ represent the variation of the data points from the lines introduced by pitching acceleration and pitching velocity, respectively.

The values of the Z_0, Z_n, $Z_{\ddot{\theta}}$, and $Z_{\dot{\theta}}$ coefficients calculated for each target are presented in tables 2, 3, 4, and 5. Table 6 lists the standard errors of the coefficients and the standard errors of estimate for each equation as calculated by the methods of reference 3 for a typical run, that is, run 15 of flight 6.

The values of the zero-lift deflection coefficient Z_0 given in table 2 are referenced to the wing zero-load position as a result of adding the wing dead weight (droop) deflections Z_i to the $Z_0 - Z_i$ coefficients. The constant Z_i for each target was determined by the use of the experimental influence coefficients for this wing which are given in reference 1 and the dead-weight distribution of figure 7 (from ref. 2). These values of Z_i are given in figure 8.

Deflection Coefficients

Examination of the Z_0 coefficients of table 2 for dissymmetry in the deflection of the right and left wing tips reveals some disagreement which is greater than the standard error of ± 0.3 inch indicated in table 6. The discrepancy between wings is concluded to be due to structural differences in the wing semispans, or perhaps to slight differences in the effective twist. As shown in figure 9 the zero-lift deflection coefficients for the various Mach numbers formed smooth continuous deflection curves when plotted against span position. In the figure it may be noted that the deflections due to the zero-lift loads are larger at the higher Mach number. This increase is not proportional to the dynamic-pressure increase, and the discrepancy is believed to be due to the effects of the L_{T_0} variation with Mach number and to possible changes in the shape of the zero-lift load distribution at the higher Mach numbers.

The Z_n coefficients presented in table 3 express the target deflections due to the additional-lift and inertia loads on the airplane per unit load factor. Examination of table 3 shows that the differences in the deflection coefficients for the right and left wings are small and in many cases within the standard error of ± 0.3 inch typical of table 6. When plotted to show the wing spar deflections due to the additional loads at the various Mach numbers, the coefficients formed smooth deflection curves as typified by figure 10. In figure 10 it is shown that the

deflection of the wing due to the additional loads decreases with Mach number. This is consistent with the inboard shift of the center of pressure on the flexible B-47A wing at the higher Mach numbers as evidenced by the wind-tunnel tests of reference 4.

Tables 4 and 5 present the target deflection coefficients associated with pitching velocity and pitching acceleration. It may be noted that the differences between right- and left-wing-tip coefficients are larger than the maximum combined standard errors of the individual wing-tip coefficients from table 6. This discrepancy suggests the possibility of small optigraph-mount twists which varied with pitching velocity and pitching acceleration or to some difference in the deflection behavior of the two wing semispans. The pitching-velocity and pitching-acceleration deflection coefficients for flight 10 are presented in figure 11 in the form of smooth spar deflection curves at various Mach numbers. The decrease with Mach number of the target deflections due to the pitching-acceleration loads, evident in the figure, may be accounted for by an examination of the term $\left(Z_{\ddot{\theta}_i} - Z_{n_{wf}} \frac{dL_T}{d\ddot{\theta}}\right)\ddot{\theta}$ in equation (3). The coefficient $Z_{n_{wf}}$ can be expected to decrease with Mach number since wind-tunnel data indicate an inward shift of the wing airload center of pressure due to flexibility effects at the higher Mach numbers. The coefficient $dL_T/d\ddot{\theta}$ may be expected to change some with Mach number since the airloads and their associated pitching moments caused by the wing deformations resulting from the pitching acceleration change with Mach number. Also, associated with the $Z_{\ddot{\theta}_i}$ deformation is a wing airload which changes with Mach number and affects the wing deformation.

In connection with the curves of figure 11 showing the wing deflections due to pitching velocity, no attempt is made to explain the differences in the deflections at the various Mach numbers, as the results shown are based on small in-flight variations and were plotted from coefficients with large standard errors.

Wing Twists

The wing twists due to the various types of loadings may be determined from the deflection coefficients given in the tables. An example of the wing twist determined from the coefficients is shown in figure 12, where the variation with Mach number of the total streamwise twist of the wing is given for an airplane load factor equal to 1. The results shown were obtained by summing the Z_0, Z_n, and Z_i coefficients for the various targets, subtracting the front- and rear-spar values, and dividing by the streamwise distances between the targets. In the figure it is evident that the variation of total wing twist with Mach number is very small. This is in agreement with the relatively small variation

of wing deflection with Mach number illustrated in figures 9, 10, and 11. Several other examples of wing twist as determined from the deflection coefficients are shown in figures 8, 13, 14, 15, and 16, where experimental and theoretical results are compared.

Comparisons

Comparisons are made in figures 13, 14, and 15 between experimental and theoretically calculated deflections and twist due to zero-lift loads, additional-lift load per unit load factor, and pitching-acceleration loads. The comparisons pertain to flight at a Mach number of 0.66, altitude of 30,000 feet, and gross weight of 108,000 pounds. This particular flight condition was selected for the comparisons in order to take partial advantage of lengthy calculations made in the early stages of the investigation. The experimental deflections and twists were obtained for this flight condition by linear interpolation of the experimental data at Mach numbers of 0.64 and 0.69 at the given weight and altitude.

In the determination of the theoretical curves of wing deflection and twist for comparison with experimental results in figures 13 to 16, the methods presented in reference 5 were used to calculate the loads acting in each case. The lift-curve slopes used in the theoretical calculations were determined with data obtained from reference 4. The wing structural-stiffness distributions were obtained from references 6 and 7. The wing deflections resulting from the application of the theoretically calculated loads were obtained through the structural influence coefficients of reference 1 and the theoretical wing twist was calculated by using the theoretical structural matrices calculated by the methods of reference 5.

In order to determine the zero-lift loads associated with figure 13, the root angle of attack was included as an unknown in equation (16) of reference 5, and an additional equation was added setting the sum of the loads on the wing and fuselage equal to the zero-lift tail load. The effects of fuselage over velocity, fuselage interference, nacelle pitching moment, wing pitching moment and nacelle thrust were included in equation (16); but the effect of nacelle interference was neglected. The fuselage was assumed to carry the same loading as the most inboard section of the wing. The tail load was calculated so as to balance the pitching moment of -0.10 at $C_L = 0$, which was obtained from reference 8. The resulting zero-lift loads were applied through the structural influence coefficients and matrices to give the calculated deflection and theoretical twist of figure 13. The discrepancies between the theoretical and experimental zero-lift deflection and twist curves, shown in figure 13, may be due to incorrect assumptions for fuselage loads, neglect of nacelle interference effects, and inaccuracy in calculated lift-curve slopes. Also, the actual deflection of the wing near the zero-load condition may not vary linearly with the load as was assumed.

The additional-lift deflection Z_n (shown in fig. 14) was determined by subtracting the theoretical zero-lift loads from the total theoretical wing load distribution calculated for the flight condition with a load factor of 2.2. The small effect of slight airplane pitching included in the original theoretical calculations was neglected. The resulting loads were reduced to a 1 g condition by dividing by the normal load factor of 2.2. These loads were applied to the wing through the structural influence coefficients of reference 1 to obtain the calculated deflections, and through the structural matrices of reference 5 to obtain the theoretical twist curve. The discrepancies between the theoretical and experimental curves shown in figure 14 are considered to be due to the same types of inaccuracies as those already mentioned in connection with the zero-lift deflection and twist curves of figure 13.

The experimental and theoretical deflections due to pitching-angular-acceleration loads are shown in figure 15 along with experimental and theoretical twist. The theoretical front-spar deflections due to pitching acceleration in figure 14 were determined by evaluating the $Z_{\ddot{\theta}_i} - Z_{n_{wf}} \frac{dL_T}{d\ddot{\theta}}$ term of equation (3). The value of $Z_{n_{wf}}$ was calculated by the methods of reference 5. The wing dead-weight distribution in figure 6 was used to calculate the inertia load due to pitching acceleration, and the tail load was calculated from the equation

$$\frac{dL_T}{d\ddot{\theta}} = \frac{I_y}{386.8 l_T}$$

where an approximate I_y was taken as $6{,}730 \times 10^6$ lb-in.^{2} as extrapolated from data of reference 9. The discrepancies between the experimental and theoretical pitching-acceleration deflection and twist shown in figure 15 are believed to be due to the neglect of the aeroelastic effects associated with the $Z_{\ddot{\theta}_i}$ coefficient, the neglect of wing airload effects on $dL_T/d\ddot{\theta}$, and the fact that the $Z_{\dot{\theta}}$ coefficients were based on small wing in-flight deflection variations of approximately 1 inch at the wing tip.

No theoretical front-spar deflections or wing twists due to pitching velocity are shown in figure 15, as it was concluded that $Z_{\dot{\theta}}$ coefficients are least accurate since examination of the standard errors of the $Z_{\dot{\theta}}$ coefficients (see table 6) shows that the twist obtained from the coefficients would have a relatively high standard error.

The comparison of experimental and theoretical wing total streamwise twist in a 2.2-load-factor pull-up at 30,000 feet showed good agreement, as is evident in figure 16. The scatter of the experimental data about the faired curve is within the band of error prescribed by the individual standard error of the coefficients.

CONCLUDING REMARKS

Experimental data have been presented which illustrate the aeroelastic behavior of the wing of the B-47A airplane. The data show that the wing deflections in the push-pull maneuver are subject to a fairly simple analysis and that they may be measured in flight with a good degree of accuracy. It is also indicated that the total twist of the wing does not change greatly with Mach number or dynamic pressure in the range used in these tests and that the theoretical calculations for the wing deflections and twist agree with experimental data.

Langley Aeronautical Laboratory,
National Advisory Committee for Aeronautics,
Langley Field, Va., November 17, 1954.

REFERENCES

1. Mayo, Alton P., and Ward, John F.: Experimental Influence Coefficients for the Deflection of the Wing of a Full-Scale, Swept-Wing Bomber. NACA RM L53L23, 1954.

2. Payne, Alan: Wing Stress Analysis. [Models XB-47 and B-47A.] Document No. D-7740 (Contract Nos. W33-038 ac 8429 and ac 22413), Boeing Airplane Co., Aug. 14, 1947.

3. Huston, Wilber B., and Skopinski, T. H.: Measurement and Analysis of Wing and Tail Buffeting Loads on a Fighter-Type Airplane. NACA TN 3080, 1954.

4. Spangler, T. A.: The Span-Load Distribution of the XB-47 Wing. Document No. D-8055, Boeing Airplane Co., Dec. 24, 1946.

5. Gray, W. L., and Schenk, K. M.: A Method for Calculating the Subsonic Stead-State Loading on an Airplane With a Wing of Arbitrary Plan Form and Stiffness. NACA TN 3030, 1953.

6. Nelson, Melvin A.: Wing Stress Analysis. [Model B-47B.] Vol. I. Document No. D-10207 (Contract No. W33-038 ac-22413), Boeing Airplane Co., April 10, 1950.

7. Parsons, Cecil E.: Wing Destruction Tests - Model B-47B. Test No. T-25299 (Contract No. W33-038 ac 22413), Boeing Airplane Co. (revised Apr. 19, 1951).

8. Van Winkle, G. Wayne: Data Report. Boeing Wind Tunnel Test No. 100 High Speed Test No. Two of the .075 Scale Three Dimensional Model of the XB-47 Airplane. Document No. D-8921, Boeing Airplane Co. Dec. 30, 1948.

9. Gray, E. Z., Sandoz, P., and Entz, H.: Design Load Criteria. [Model B-47B.] Vol. I. Document No. D-9441 (Contract No. W33-038 ac-22413), Boeing Airplane Co., Nov. 9, 1948.

TABLE 1.- FLIGHT CONDITIONS

Flight	Run	Mach number	Airplane weight, lb	Altitude, ft	Dynamic pressure, q, lb/sq ft	Center of gravity, percent M.A.C.
3	11	0.74	120,300	35,000	196	13.65
4	19	.70	108,900	25,000	265	20.97
4	20	.60	108,700	25,000	189	20.91
4	21	.51	108,400	25,000	128	20.85
6	12	.78	108,700	30,000	267	13.10
6	13	.74	108,400	30,000	244	13.12
6	14	.69	108,200	30,000	215	13.16
6	15	.64	107,600	30,000	187	13.03
9	2	.64	126,200	35,000	146	22.55
9	3	.68	126,100	35,000	161	22.66
9	4	.72	125,700	35,000	185	22.91
9	5	.76	125,400	35,000	214	23.12
9	6	.78	125,200	35,000	217	23.28
10	3	.60	127,200	30,000	159	22.64
10	5	.68	126,300	30,000	200	22.39
10	6	.72	126,100	30,000	230	22.51
10	7	.76	125,400	30,000	255	22.96
10	9	.80	124,900	30,000	275	23.28

TABLE 2.- ZERO-LIFT WING DEFLECTION COEFFICIENT, Z_0

Flight	Run	Zero-lift wing deflection coefficient, in., at target* -											
		5	6	7	8	9	10	11	12	13	14	15	16
3	11	----	----	----	----	8.75	9.22	5.38	5.98	----	----	1.37	----
4	19	8.89	----	4.68	5.07	6.87	----	4.50	4.96	2.38	3.04	.94	----
4	20	7.76	----	4.02	4.36	6.22	----	3.93	4.09	2.13	2.77	1.02	----
4	21	7.22	----	3.60	4.38	6.16	----	3.67	4.61	1.87	2.78	.47	----
6	12	10.53	9.20	5.12	6.21	7.69	8.23	4.98	5.08	2.82	3.51	1.21	1.35
6	13	10.48	8.55	5.06	6.79	7.66	7.65	4.95	5.11	3.19	3.70	1.77	1.82
6	14	9.47	7.11	4.50	5.94	6.46	6.71	4.09	4.41	2.63	3.35	1.46	1.58
6	15	8.04	6.32	3.65	5.41	5.96	5.97	3.63	3.66	2.48	2.86	1.43	1.33
9	2	9.62	----	4.35	4.88	8.73	8.90	4.84	5.11	2.43	3.21	.90	.86
9	3	9.77	----	4.54	4.99	8.79	8.68	4.80	4.97	2.41	3.07	.86	.93
9	4	11.60	----	5.86	6.59	10.45	11.18	5.82	6.47	2.96	4.00	1.04	1.41
9	5	11.16	----	5.50	5.76	10.23	10.00	5.65	5.66	2.95	3.42	.93	.79
9	6	11.91	----	5.95	6.20	10.24	10.10	5.81	5.76	2.83	3.38	.60	1.05
10	3	6.64	5.98	2.96	3.80	7.78	8.34	3.86	4.36	2.01	2.83	.93	----
10	5	8.40	7.57	3.91	4.46	8.30	8.87	4.20	4.93	2.14	3.04	.93	----
10	6	9.51	8.85	4.51	5.16	7.92	8.31	4.19	4.65	2.01	2.87	.71	----
10	7	9.08	8.19	4.38	5.07	9.22	9.99	5.01	5.65	2.42	3.35	.88	----
10	9	11.72	11.10	5.40	6.61	10.46	11.12	5.72	6.29	2.36	3.32	1.03	----

*Dashes mean target lamp was out during run.

TABLE 3.- ADDITIONAL-LIFT WING DEFLECTION COEFFICIENT, Z_n

Flight	Run	Additional-lift wing deflection coefficient, in./n, at target* -											
		5	6	7	8	9	10	11	12	13	14	15	16
3	11	----	----	----	----	22.63	23.60	13.74	14.28	----	----	1.42	----
4	19	19.90	----	12.13	13.48	20.76	----	12.39	13.32	6.67	7.80	1.41	----
4	20	21.03	----	12.73	14.18	21.60	----	12.96	14.26	6.89	8.03	1.33	----
4	21	21.73	----	13.19	13.99	22.07	----	13.49	13.82	7.26	8.01	1.99	----
6	12	19.16	20.08	11.69	12.86	19.70	20.41	11.70	12.69	6.32	7.38	1.39	2.22
6	13	18.73	20.32	11.45	12.82	19.16	20.52	11.43	12.29	5.81	7.03	.87	1.76
6	14	21.35	19.41	11.82	13.33	20.32	21.31	12.17	12.89	6.26	7.25	1.15	1.88
6	15	20.96	22.23	12.68	13.89	20.55	21.77	12.50	13.48	6.30	7.58	1.14	2.11
9	2	25.20	----	15.43	16.82	25.03	26.45	14.99	15.94	8.12	9.36	1.88	2.68
9	3	25.09	----	15.21	16.75	24.80	26.62	14.99	16.06	8.14	9.50	1.91	2.48
9	4	22.66	----	13.63	14.82	22.61	23.35	13.71	14.23	7.43	8.35	1.68	2.04
9	5	22.99	----	13.96	15.68	22.86	24.75	13.95	15.23	7.51	9.14	1.80	2.75
9	6	22.38	----	13.62	15.37	22.69	24.45	13.72	15.06	7.58	9.12	2.17	2.50
10	3	27.75	28.94	16.57	17.68	25.82	26.89	15.75	16.60	8.05	9.32	1.60	----
10	5	25.57	26.86	16.91	15.45	24.82	25.79	15.04	15.81	7.86	9.08	1.64	----
10	6	24.31	25.43	14.82	16.20	24.69	25.83	15.03	15.86	7.90	9.14	1.84	----
10	7	24.58	25.87	14.91	16.20	23.51	24.27	14.28	14.93	7.55	8.70	1.67	----
10	9	24.58	24.55	13.50	14.65	22.70	23.56	13.85	14.56	7.22	8.34	1.54	----

*Dashes mean target lamp was out during run.

TABLE 4.- PITCHING-ACCELERATION WING DEFLECTION COEFFICIENT, $Z_{\ddot{\theta}}$

Flight	Run	Pitching-acceleration wing deflection coefficient, in./radians/sec^2, at target* -											
		5	6	7	8	9	10	11	12	13	14	15	16
3	11	----	----	----	----	7.34	10.26	5.48	5.31	----	----	-2.53	----
4	19	10.07	----	5.82	7.76	10.12	----	6.18	7.87	3.19	5.07	-.58	----
4	20	11.58	----	6.77	8.44	11.54	----	7.12	9.16	3.27	4.53	-.40	----
4	21	12.69	----	7.68	7.06	12.57	----	8.67	7.93	4.55	4.60	1.78	----
6	12	10.84	12.51	6.99	7.70	10.55	12.30	5.98	8.39	3.63	5.17	.86	1.39
6	13	8.71	11.38	5.49	6.79	8.25	10.80	4.80	6.02	2.00	3.28	-.85	-.31
6	14	11.41	15.62	6.89	8.39	11.53	14.27	7.54	8.02	3.18	4.22	.04	.23
6	15	15.52	17.93	9.18	10.41	12.90	15.56	8.36	9.98	3.85	4.71	-.10	1.40
9	2	10.59	----	7.06	7.76	9.25	12.25	5.58	6.93	2.84	3.29	.62	.85
9	3	10.16	----	5.95	7.21	9.18	13.23	5.53	7.34	3.11	4.27	.69	.03
9	4	7.31	----	3.16	3.73	5.60	6.67	3.48	3.73	1.68	1.83	.29	-.43
9	5	9.97	----	4.79	7.23	6.94	12.03	4.89	7.33	2.12	4.92	.64	1.44
9	6	6.67	----	3.65	6.41	6.56	11.21	3.88	6.98	2.42	4.50	2.62	.75
10	3	20.00	21.47	10.97	10.77	12.36	13.85	7.94	8.91	3.13	4.31	-.45	----
10	5	14.81	17.18	8.86	10.51	11.23	13.21	6.98	8.08	3.42	4.79	.28	----
10	6	12.51	15.18	7.73	9.64	12.11	15.27	7.88	9.15	3.65	5.25	.69	----
10	7	14.71	18.42	8.94	10.10	10.32	11.89	6.11	7.16	2.68	4.30	.18	----
10	9	7.06	9.46	4.97	5.93	8.37	10.41	5.17	6.55	2.29	3.34	-.02	----

*Dashes mean target lamp was out during run.

TABLE 5.- PITCHING-VELOCITY WING DEFLECTION COEFFICIENT, $Z_{\dot{\theta}}$

Flight	Run	Pitching-velocity wing deflection coefficient, in./radians/sec, at target* -											
		5	6	7	8	9	10	11	12	13	14	15	16
3	11	----	----	----	----	-3.33	2.42	-1.09	-0.01	----	----	.72	----
4	19	9.11	----	4.94	.35	-8.64	----	-3.01	-4.92	-1.69	-3.71	-.50	----
4	20	4.21	----	2.72	-1.46	-5.11	----	-2.40	-4.70	-.76	-1.12	.19	----
4	21	8.48	----	4.86	3.64	1.52	----	.93	1.72	.45	1.04	-1.24	----
6	12	8.93	5.49	4.53	-.08	-6.43	-.50	-2.60	-3.63	-1.53	-2.21	-.34	-1.36
6	13	8.12	7.25	4.36	5.29	-3.85	.13	-1.09	-1.23	.17	-.69	.24	.98
6	14	6.63	2.26	3.59	-.03	-3.63	-.12	-1.04	-1.18	.51	.01	.85	-.01
6	15	-2.51	-3.11	1.61	-3.43	-4.66	-1.35	-1.84	-2.74	.20	-1.38	.65	-.16
9	2	4.50	----	2.58	.37	-1.02	.81	.15	-.48	.25	.05	.40	.66
9	3	3.36	----	2.43	-.07	-2.84	-.31	-1.19	-1.53	-.87	-1.18	-.89	-.52
9	4	5.82	----	5.09	2.44	.33	5.49	.82	1.74	.48	.99	.41	1.46
9	5	4.65	----	4.12	-1.25	-3.54	-1.22	-1.68	-.28	.02	-1.91	-.12	.55
9	6	9.04	----	6.57	1.20	-2.61	.32	.38	-2.12	-1.43	-3.37	-1.27	-.77
10	3	1.95	3.36	1.07	1.71	-5.96	-2.36	-2.98	-3.07	-1.02	-1.21	-.34	----
10	5	4.44	6.38	2.73	1.68	-4.32	-.09	-1.98	-1.61	.12	-.49	.37	----
10	6	3.84	5.07	2.15	.42	-7.64	-3.01	-3.99	-3.95	-1.13	-2.38	-.55	----
10	7	3.38	.96	1.69	.19	-8.61	-2.30	-4.01	-3.33	-1.42	-1.79	.09	----
10	9	5.76	4.46	2.55	-.25	-11.81	-5.10	-6.23	-5.03	-2.60	-2.84	-1.35	----

*Dashes mean target lamp was out during run.

TABLE 6.- TYPICAL STANDARD-ERROR LISTING FOR FLIGHT 6, RUN 15

Target	Target deflections and standard errors								
	S_Z	Z_0	S_{Z_0}	Z_n	S_{Z_n}	$Z_{\ddot{\theta}}$	$S_{Z_{\ddot{\theta}}}$	$Z_{\dot{\theta}}$	$S_{Z_{\dot{\theta}}}$
5	±0.15	20.90	±0.30	20.96	±0.33	15.52	±1.15	-2.51	±1.39
6	±.15	19.76	±.31	22.23	±.33	17.93	±1.17	-3.11	±1.41
7	±.09	11.40	±.18	12.68	±.19	9.18	±.68	1.61	±.81
8	±.06	13.45	±.13	13.89	±.15	10.41	±.52	-3.43	±.62
9	±.15	18.82	±.30	20.55	±.31	12.90	±1.12	-4.66	±1.35
10	±.12	19.41	±.24	21.77	±.25	15.56	±.93	-1.35	±1.13
11	±.10	11.38	±.21	12.50	±.22	8.36	±.81	-1.84	±.98
12	±.07	11.70	±.15	13.48	±.15	9.98	±.53	-2.74	±.65
13	±.07	6.86	±.16	6.30	±.18	3.85	±.62	.20	±.74
14	±.07	7.28	±.15	7.58	±.15	4.71	±.55	-1.38	±.65
15	±.06	2.41	±.13	1.14	±.15	-.10	±.50	.65	±.62
16	±.04	2.65	±.09	2.11	±.09	1.40	±.33	-.16	±.39

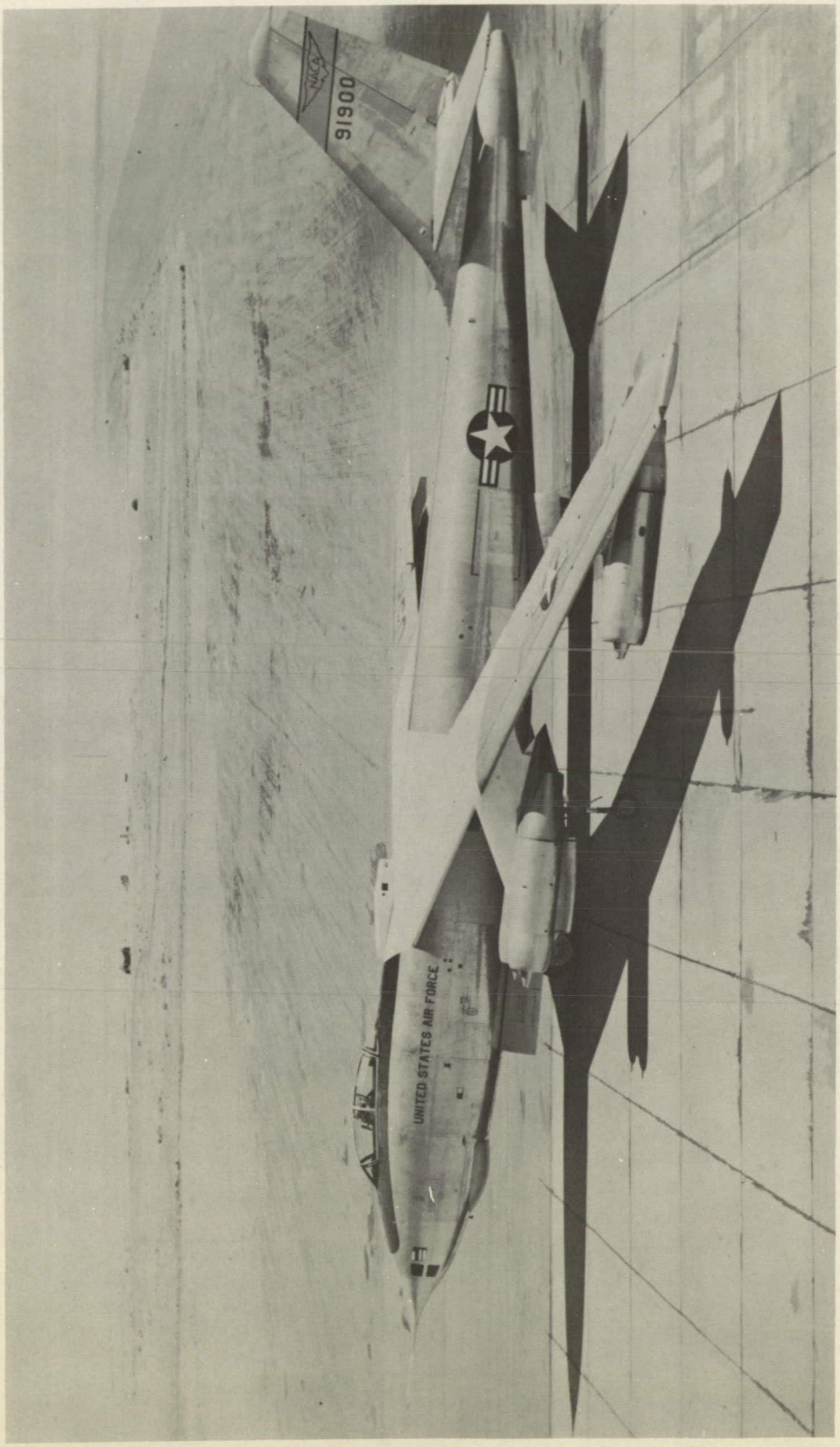

L-86692

Figure 1.- Photograph of the test airplane.

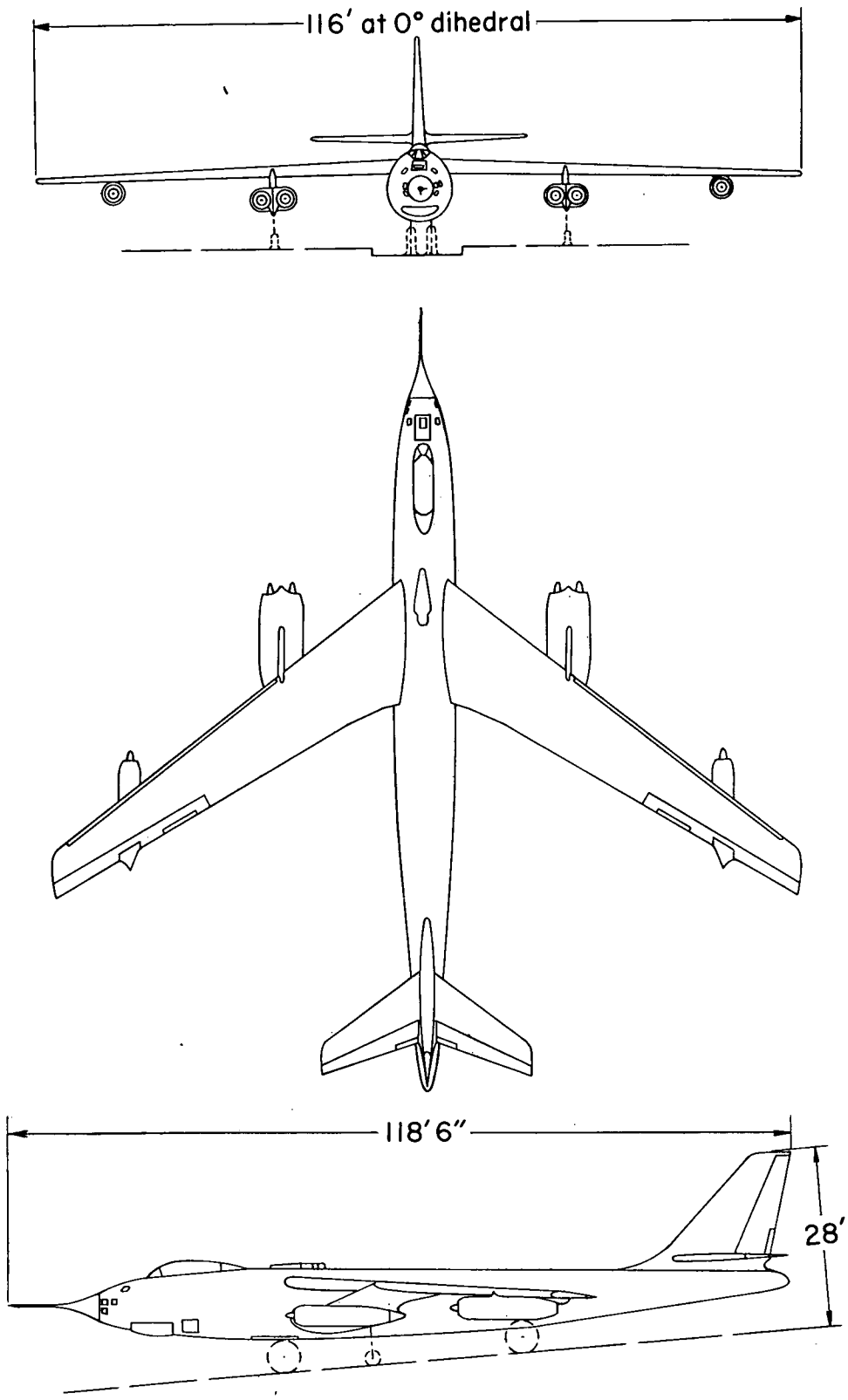

Figure 2.- Three views of test airplane.

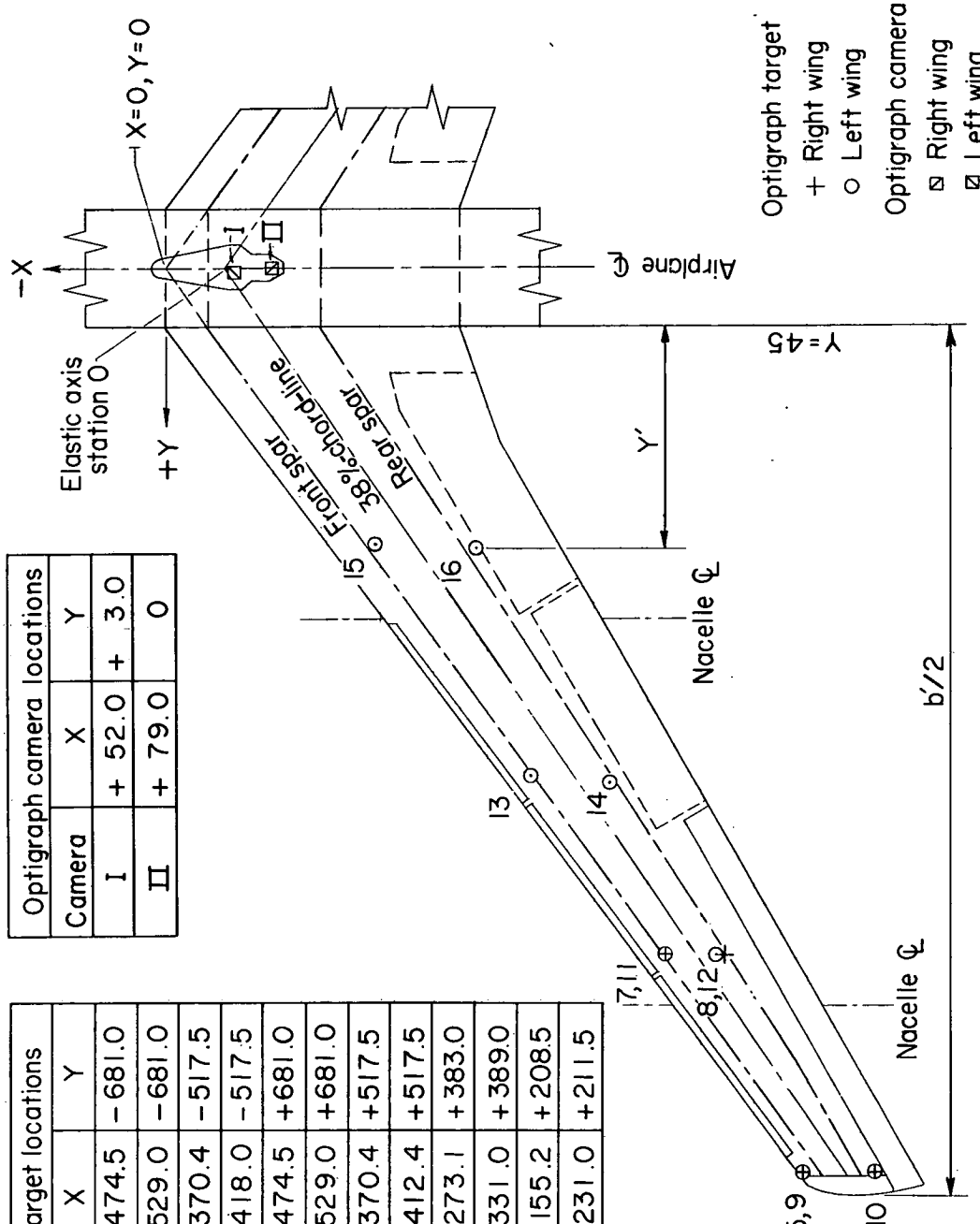

Optigraph camera locations		
Camera	X	Y
I	+ 52.0	+ 3.0
II	+ 79.0	0

Optigraph target locations		
Target no.	X	Y
5	+474.5	-681.0
6	+529.0	-681.0
7	+370.4	-517.5
8	+418.0	-517.5
9	+474.5	+681.0
10	+529.0	+681.0
11	+370.4	+517.5
12	+412.4	+517.5
13	+273.1	+383.0
14	+331.0	+389.0
15	+155.2	+208.5
16	+231.0	+211.5

All dimensions are given in inches

Figure 3.- Location of optigraph cameras and targets used during test.

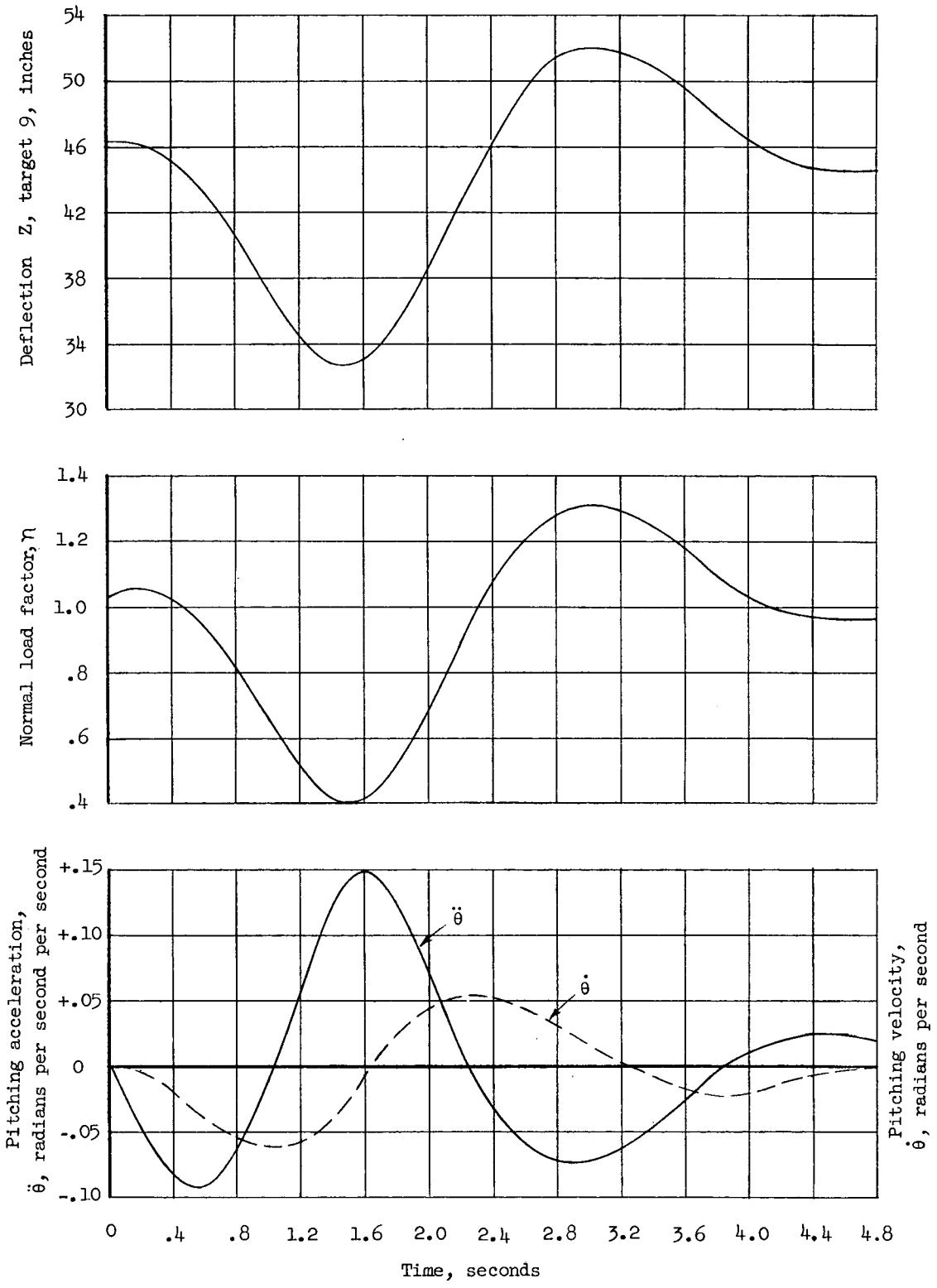

Figure 4.- Typical time-history data of a push-pull maneuver. Altitude, 30,000 feet; Mach number, 0.72; airplane weight, 126,000 pounds.

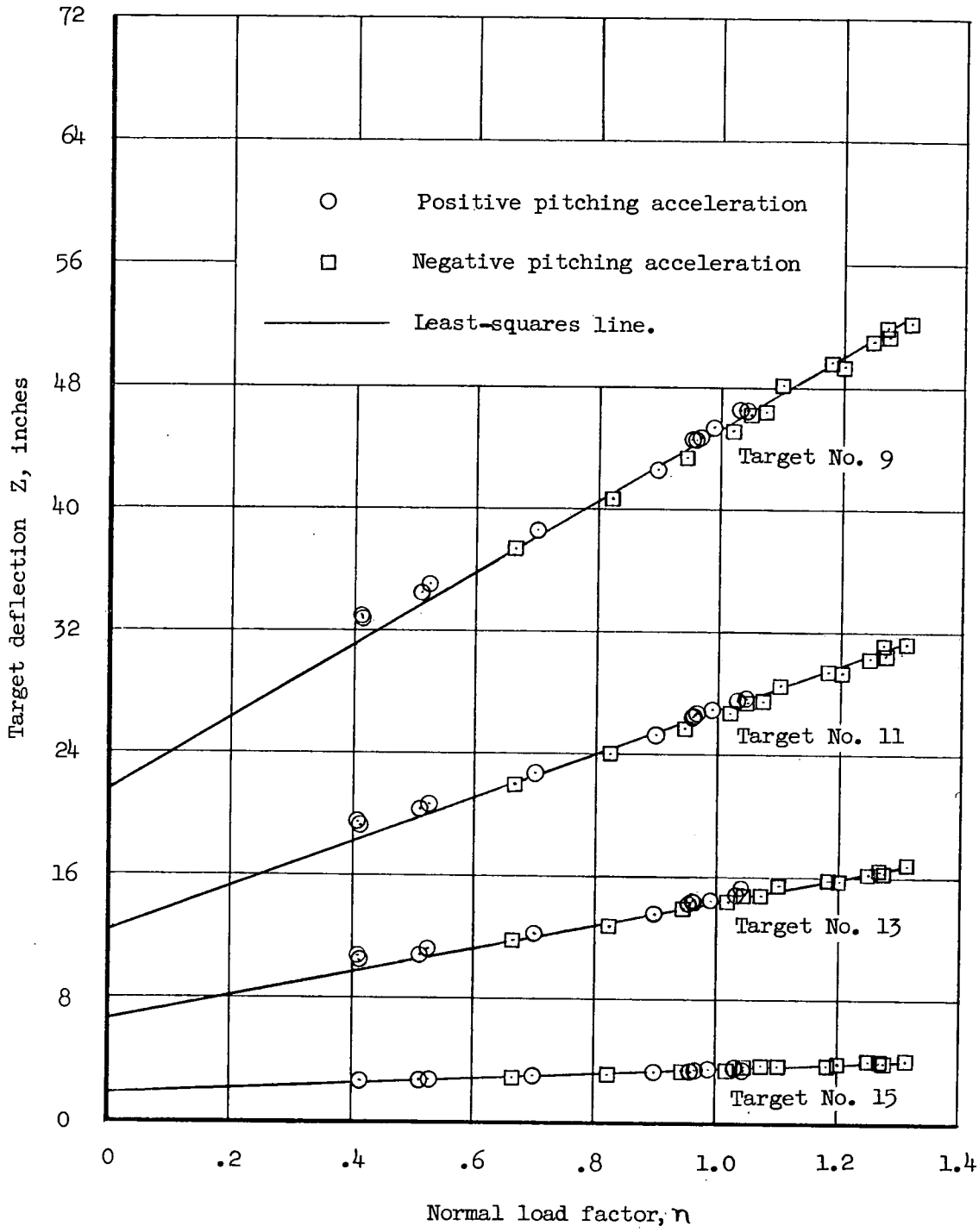

Figure 5.- Typical variation of target deflections with normal load factor. Altitude, 30,000 feet; Mach number, 0.72; airplane weight, 126,000 pounds.

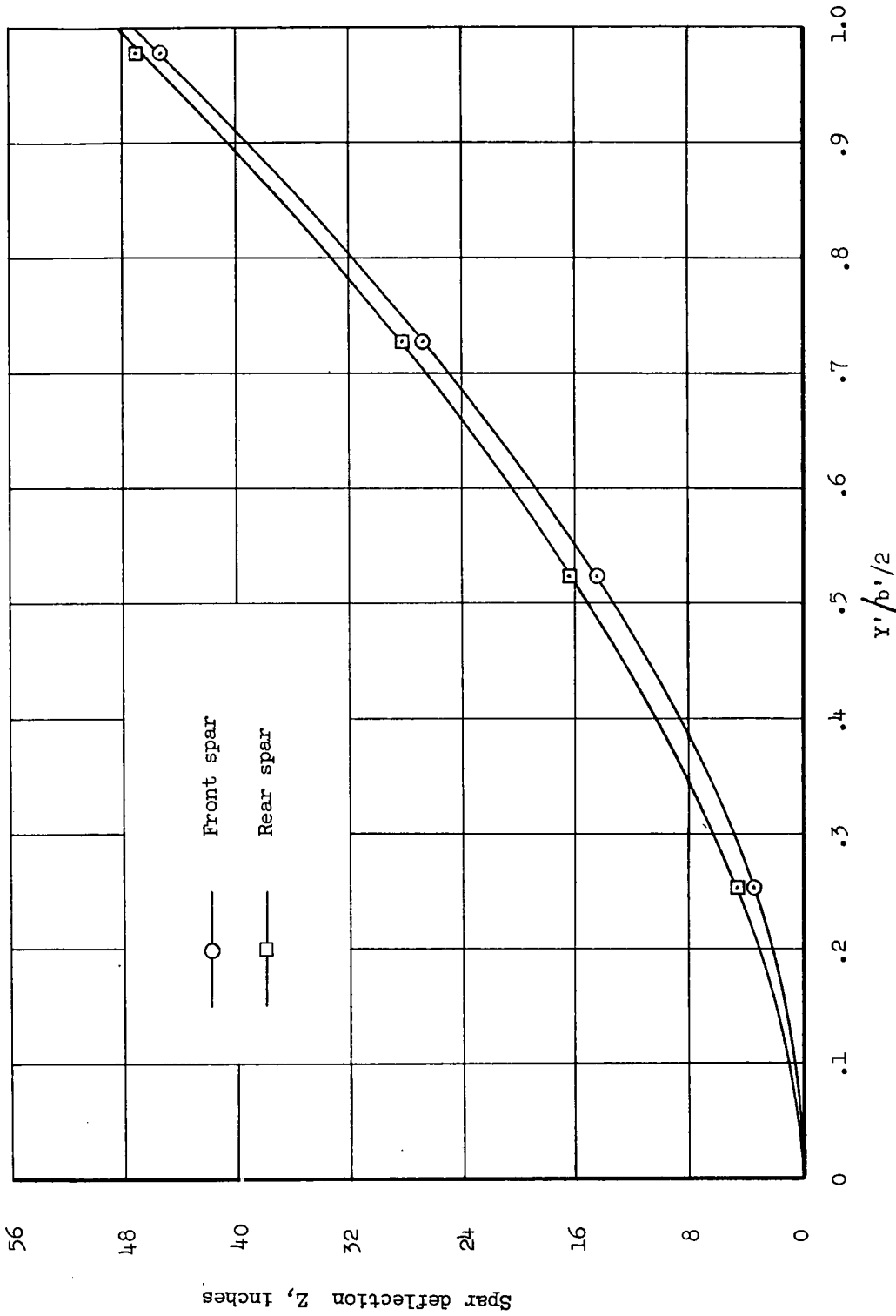

Figure 6.- Typical spar deflection curve. Altitude, 35,000 feet; Mach number, 0.72; load factor, 1; airplane weight, 126,000 pounds.

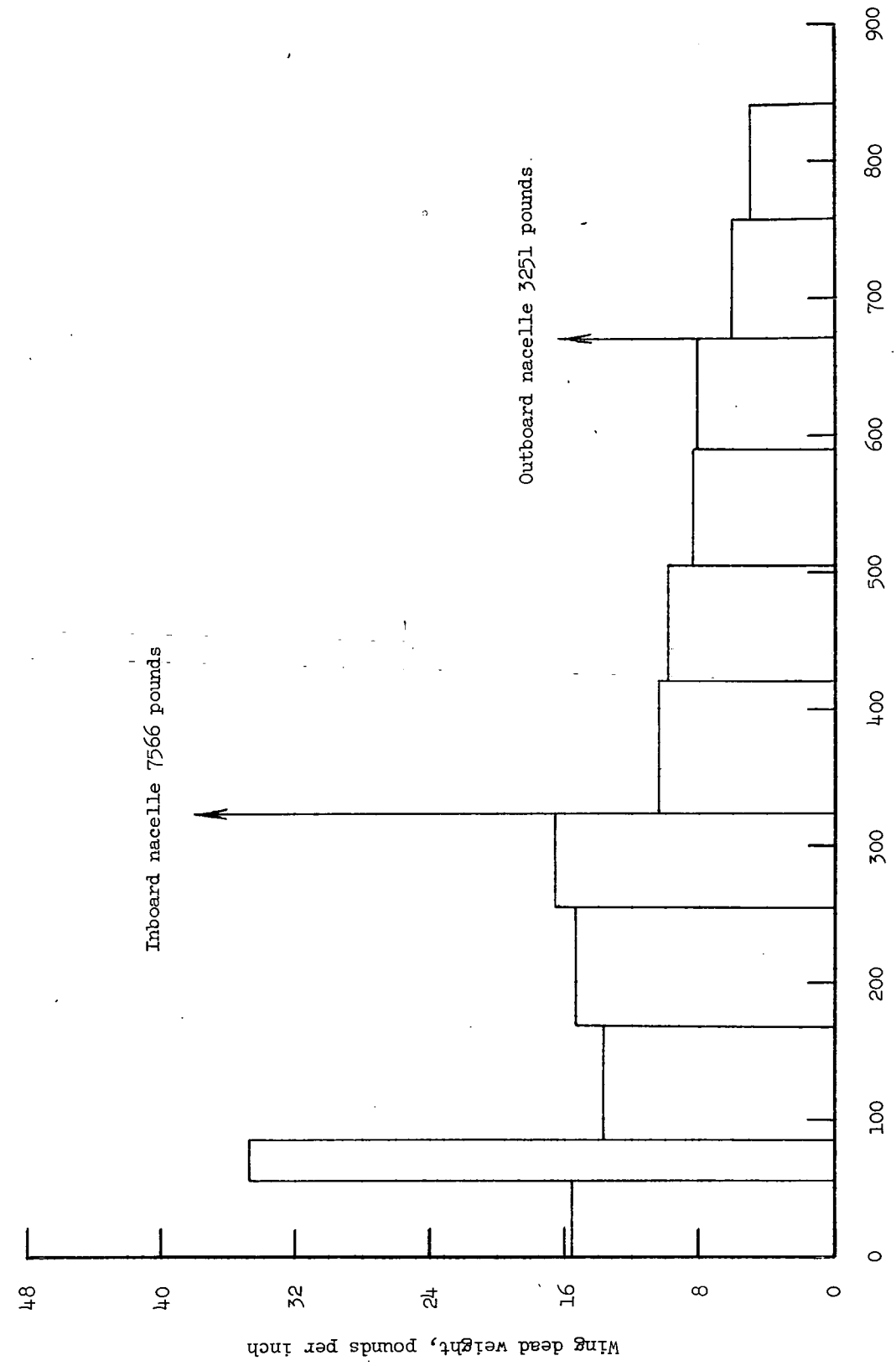

Figure 7.- Wing dead-weight distribution and nacelle loads (from ref. 2).

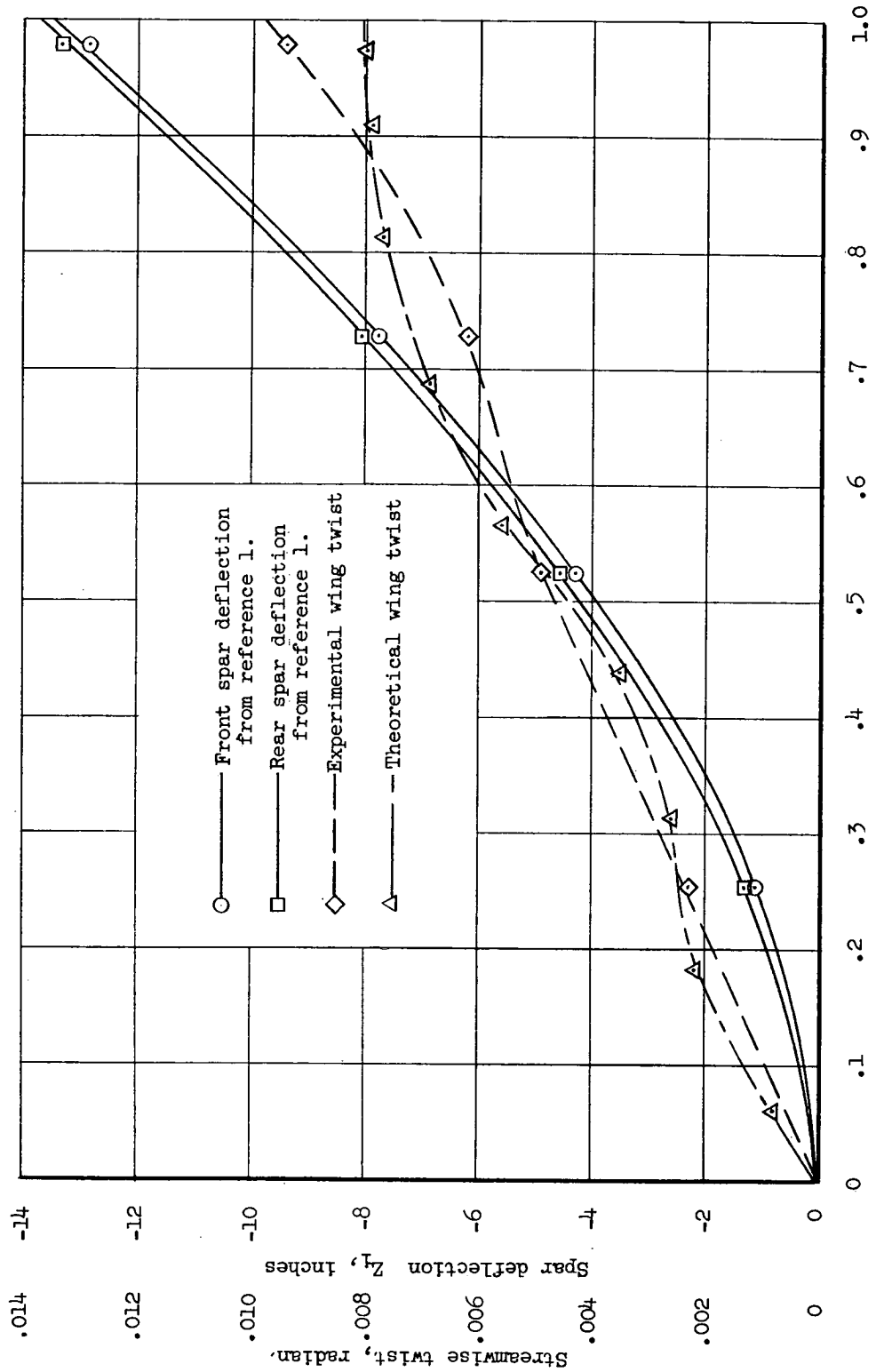

Figure 8.- Spar deflection and streamwise twist due to wing and nacelle dead weight.

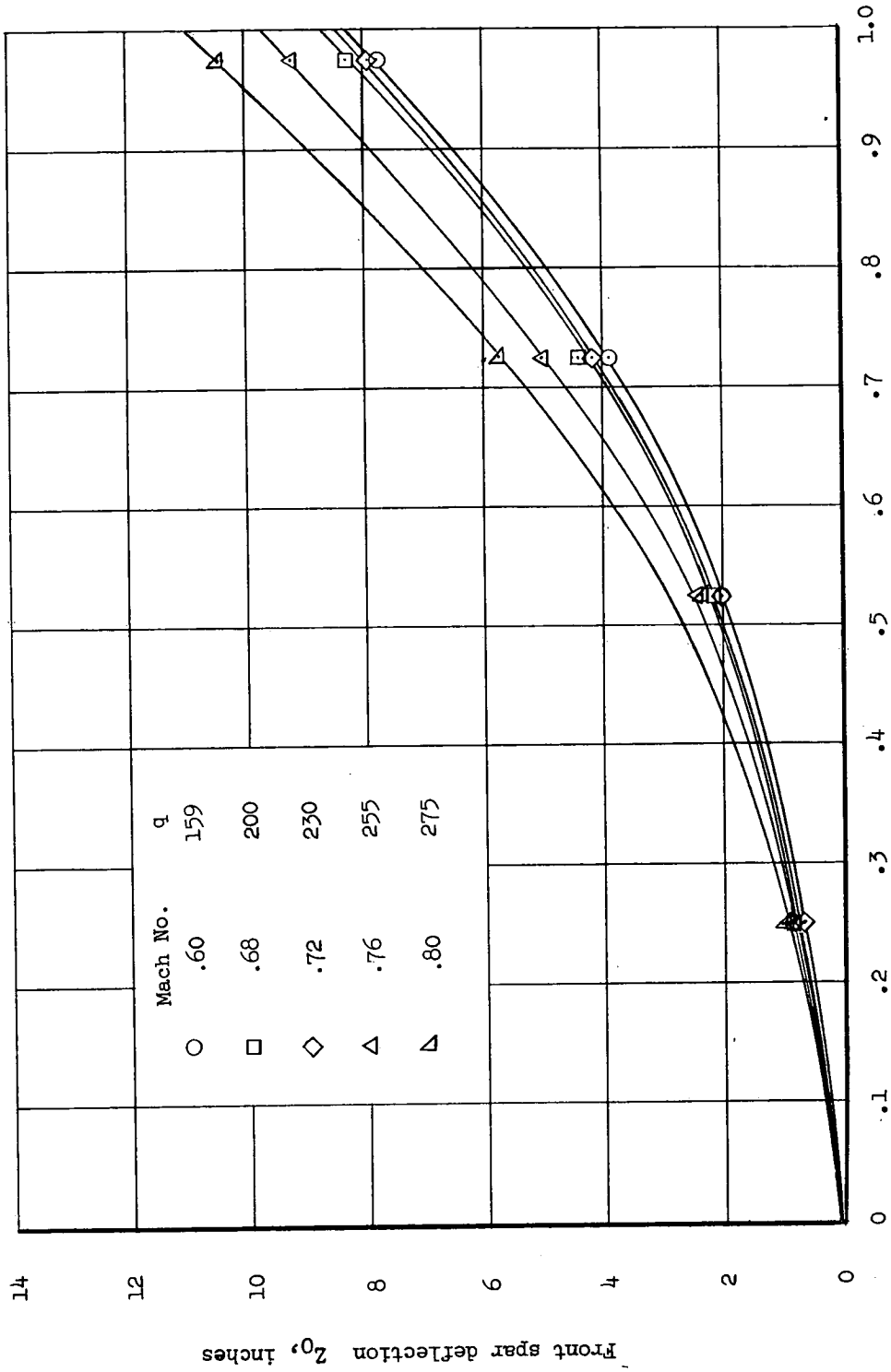

Figure 9.- Front spar deflections, at various Mach numbers, due to zero-lift loads. Altitude, 30,000 feet; airplane weight, 126,000 pounds.

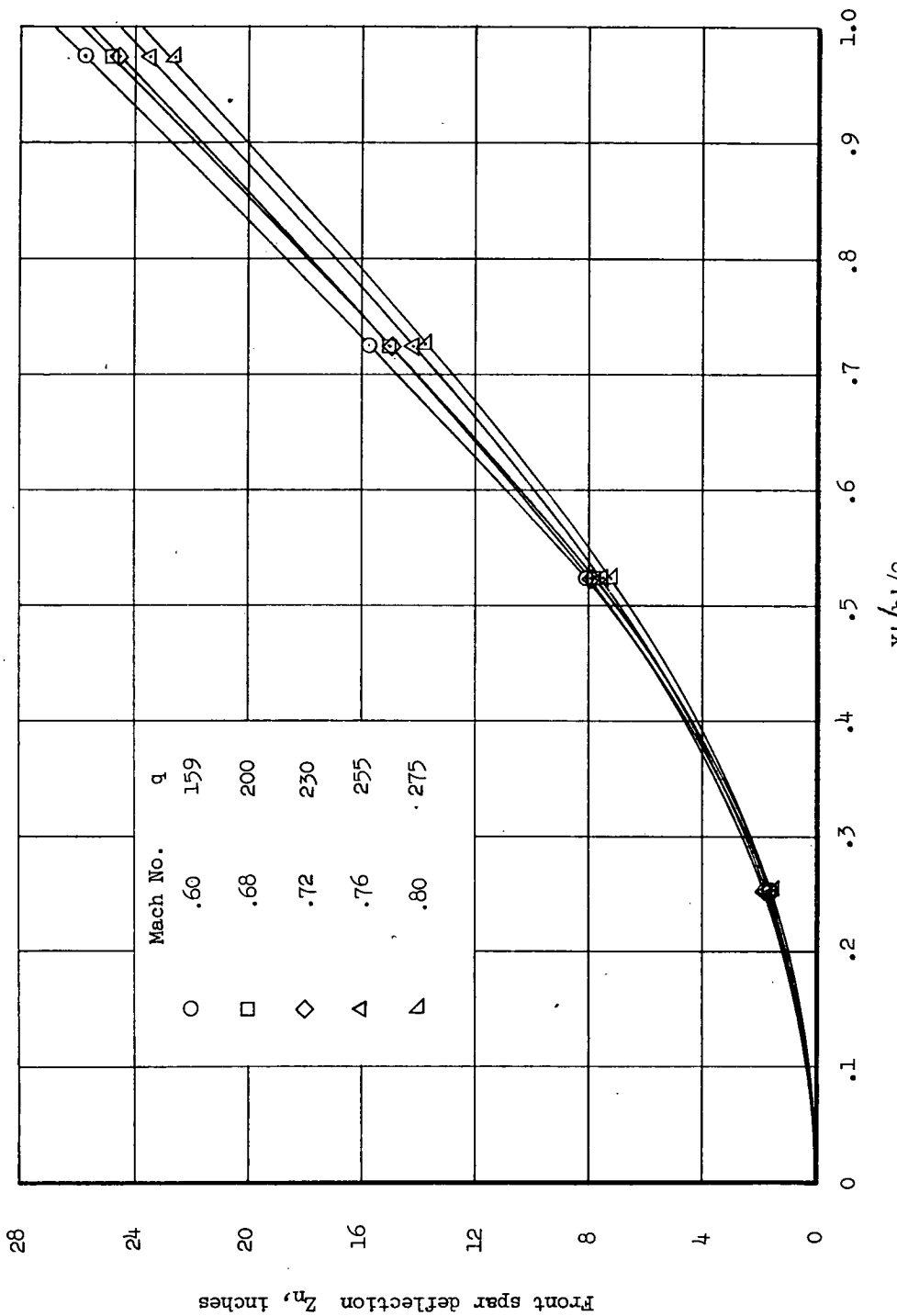

Figure 10.- Front spar deflections, at various Mach numbers, due to additional-lift load per unit load factor. Altitude, 30,000 feet; airplane weight, 126,000 pounds.

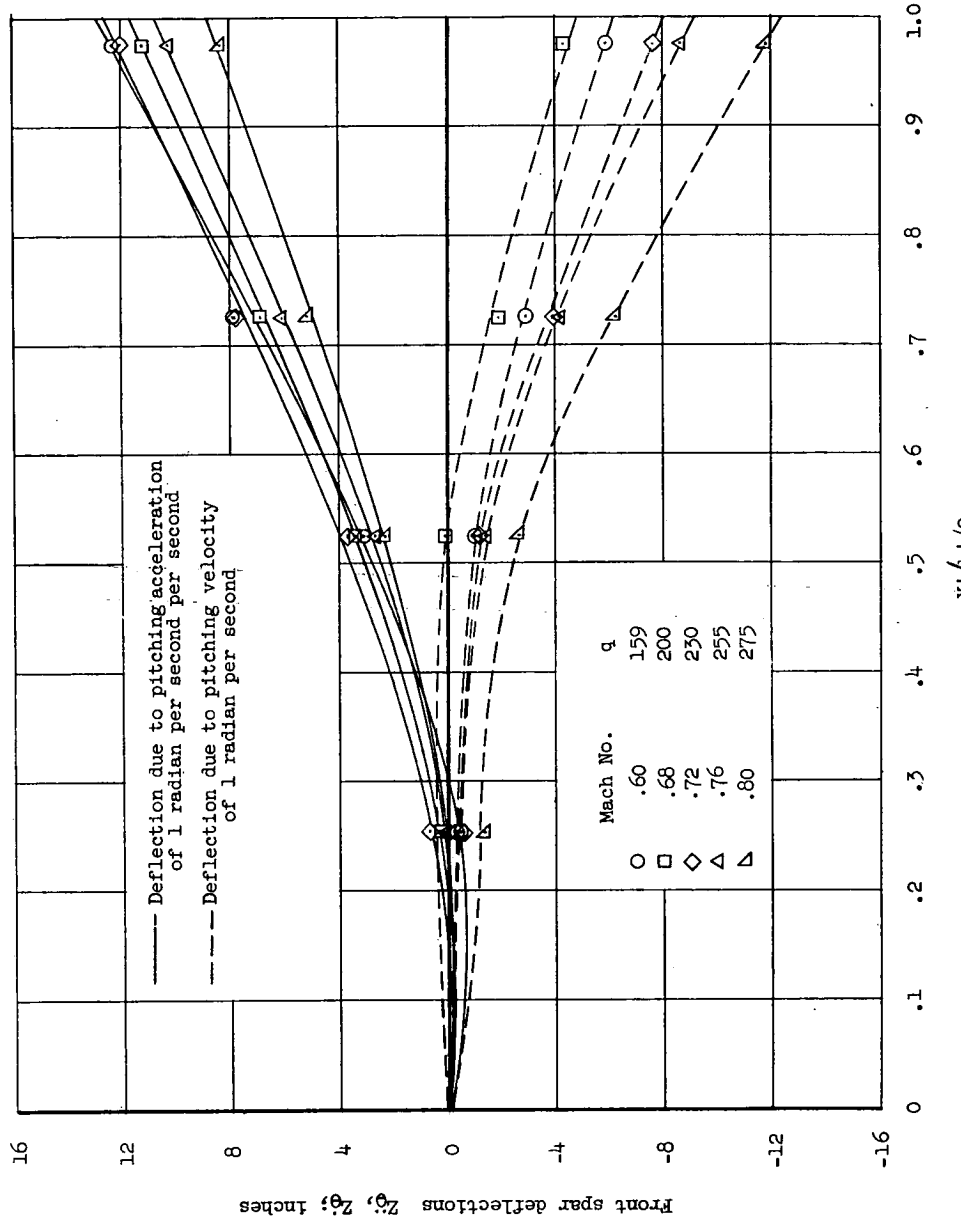

Figure 11.- Front spar deflections, at various Mach numbers, due to pitching-acceleration loads and pitching-velocity loads. Altitude, 30,000 feet; airplane weight, 126,000 pounds.

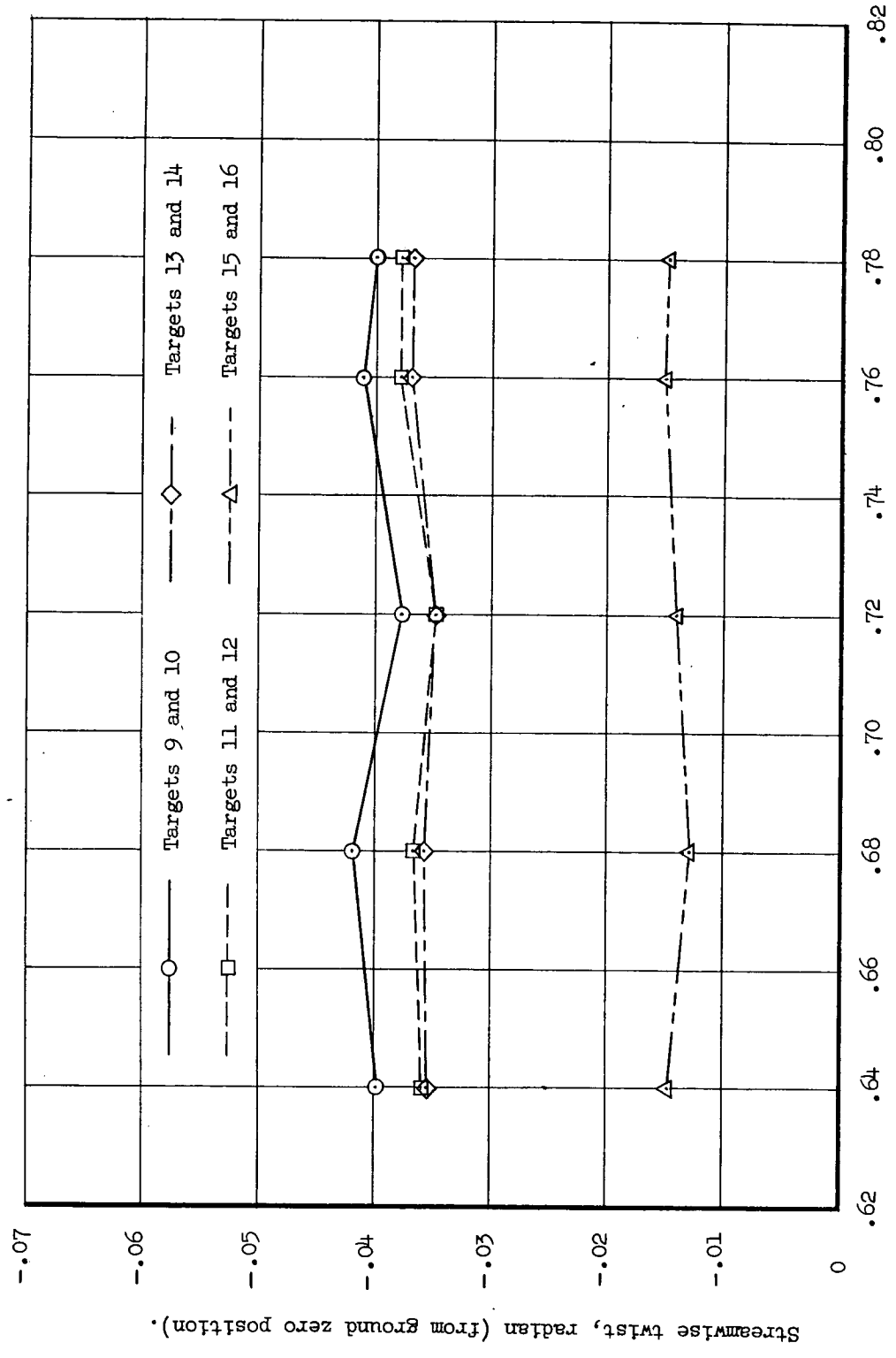

Figure 12.- Typical wing twist variation with Mach number. Altitude, 35,000 feet; airplane weight, 126,000 pounds; $n = 1$; $\dot{\theta} = 0$; $\ddot{\theta} = 0$.

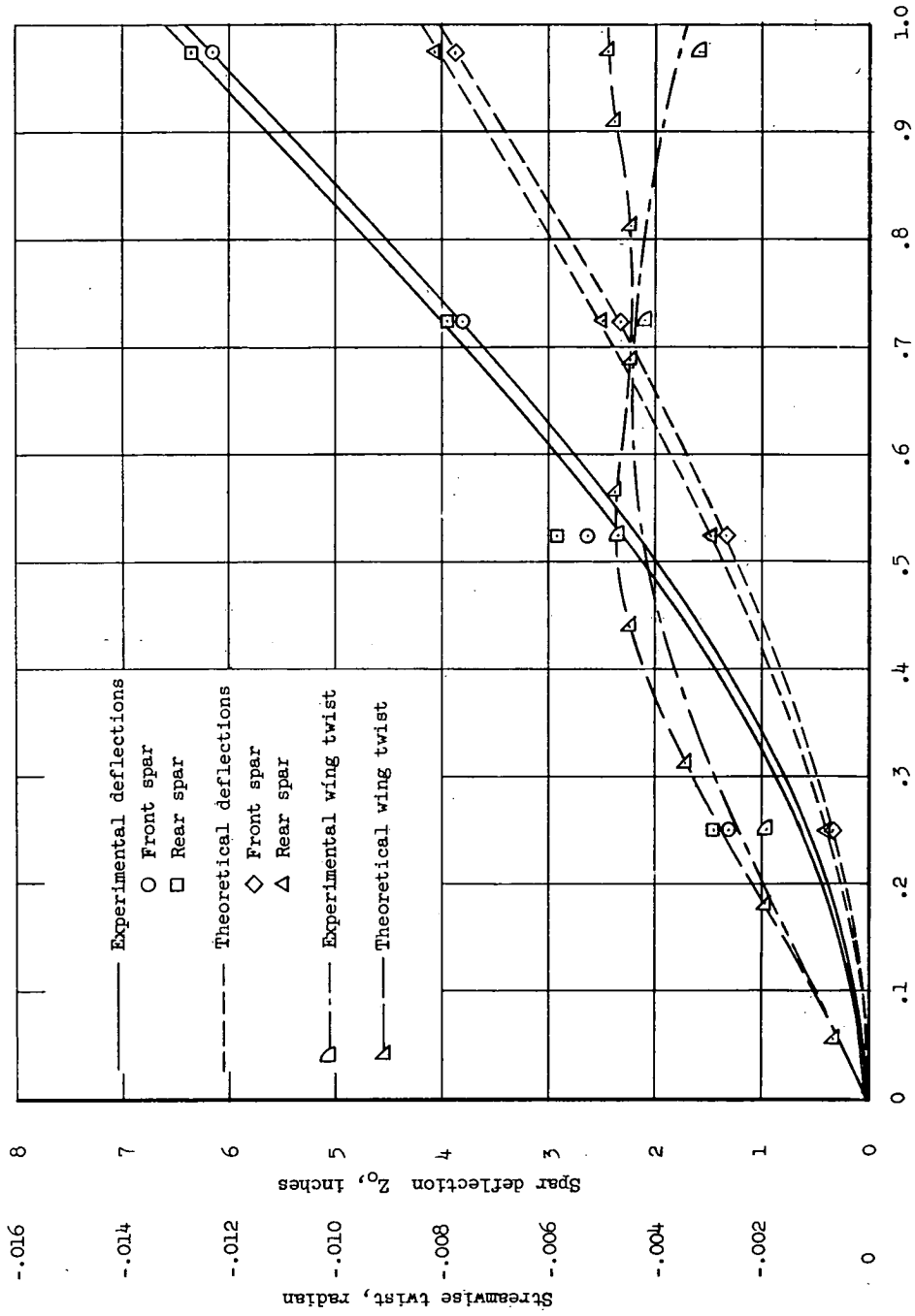

Figure 13.- Comparison of theoretical and experimental spar deflections and wing twist due to zero-lift loads. Altitude, 30,000 feet; Mach number, 0.66; airplane weight, 108,000 pounds.

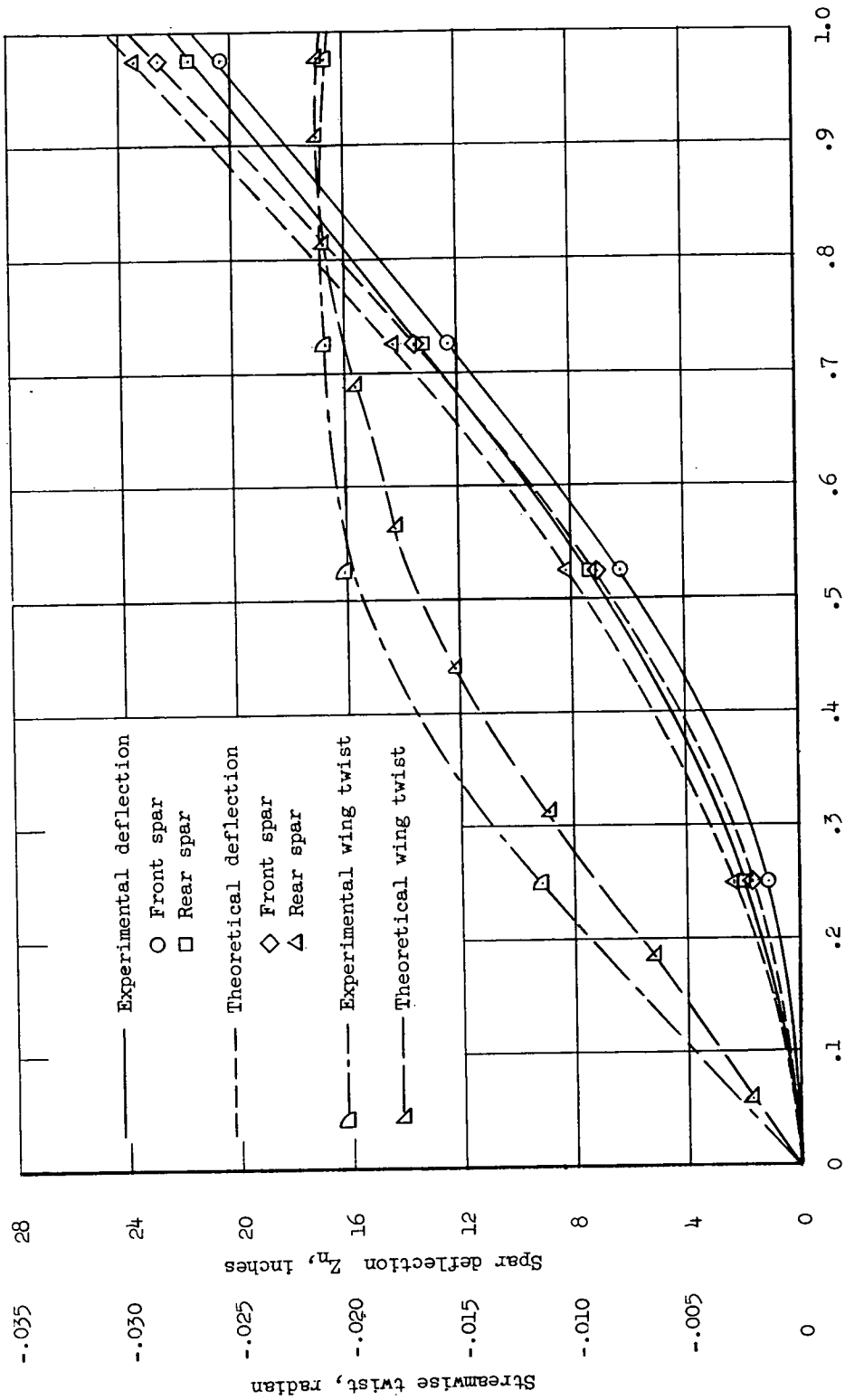

Figure 14.- Comparison of theoretical and experimental spar deflections and wing twist due to additional-lift load per unit load factor. Altitude, 30,000 feet; Mach number, 0.66; airplane weight, 108,000 pounds.

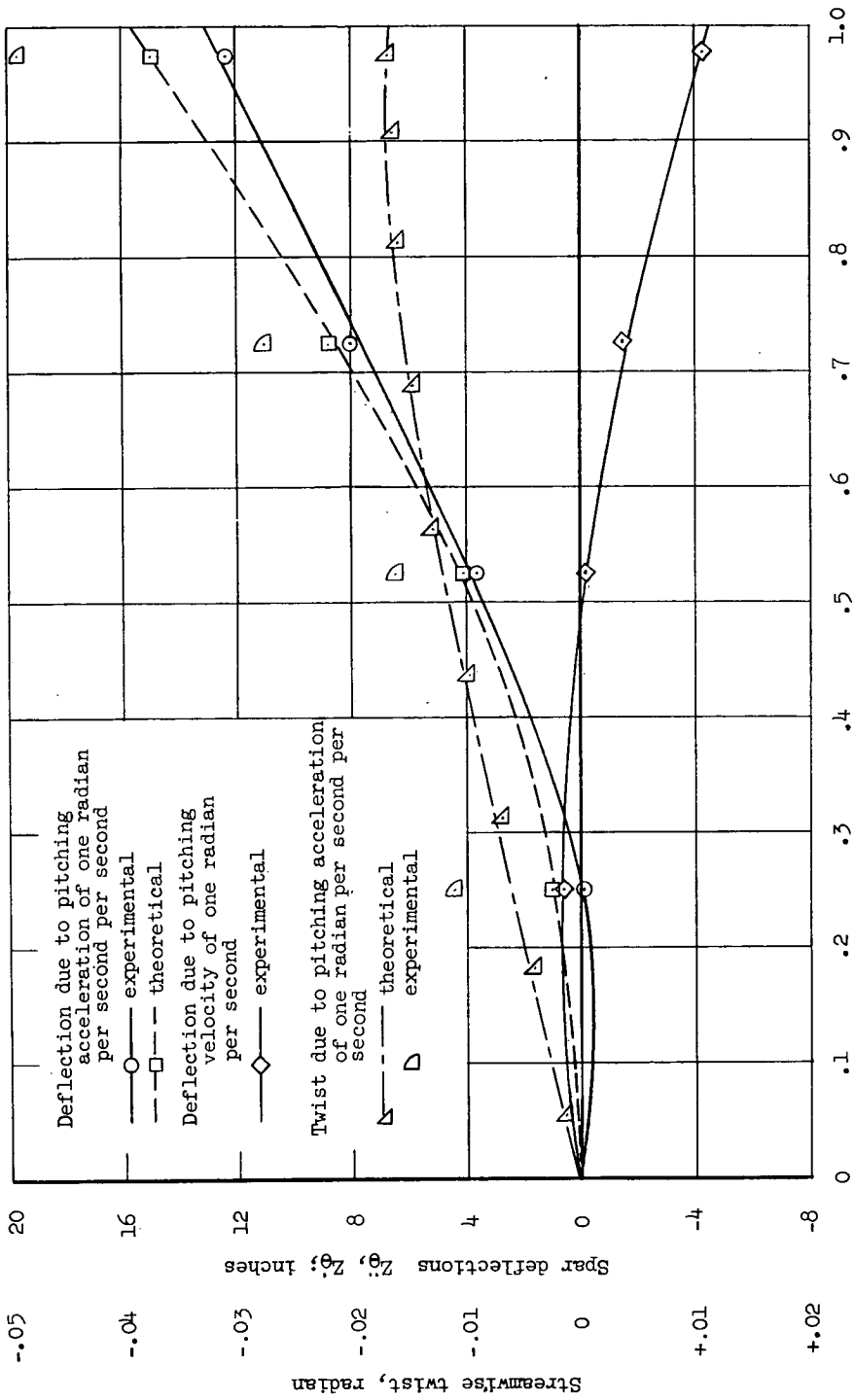

Figure 15.- Comparison of theoretical and experimental front spar deflections and wing twist due to pitching-acceleration loads and pitching-velocity loads. Altitude, 30,000 feet; Mach number, 0.66; airplane weight, 108,000 pounds.

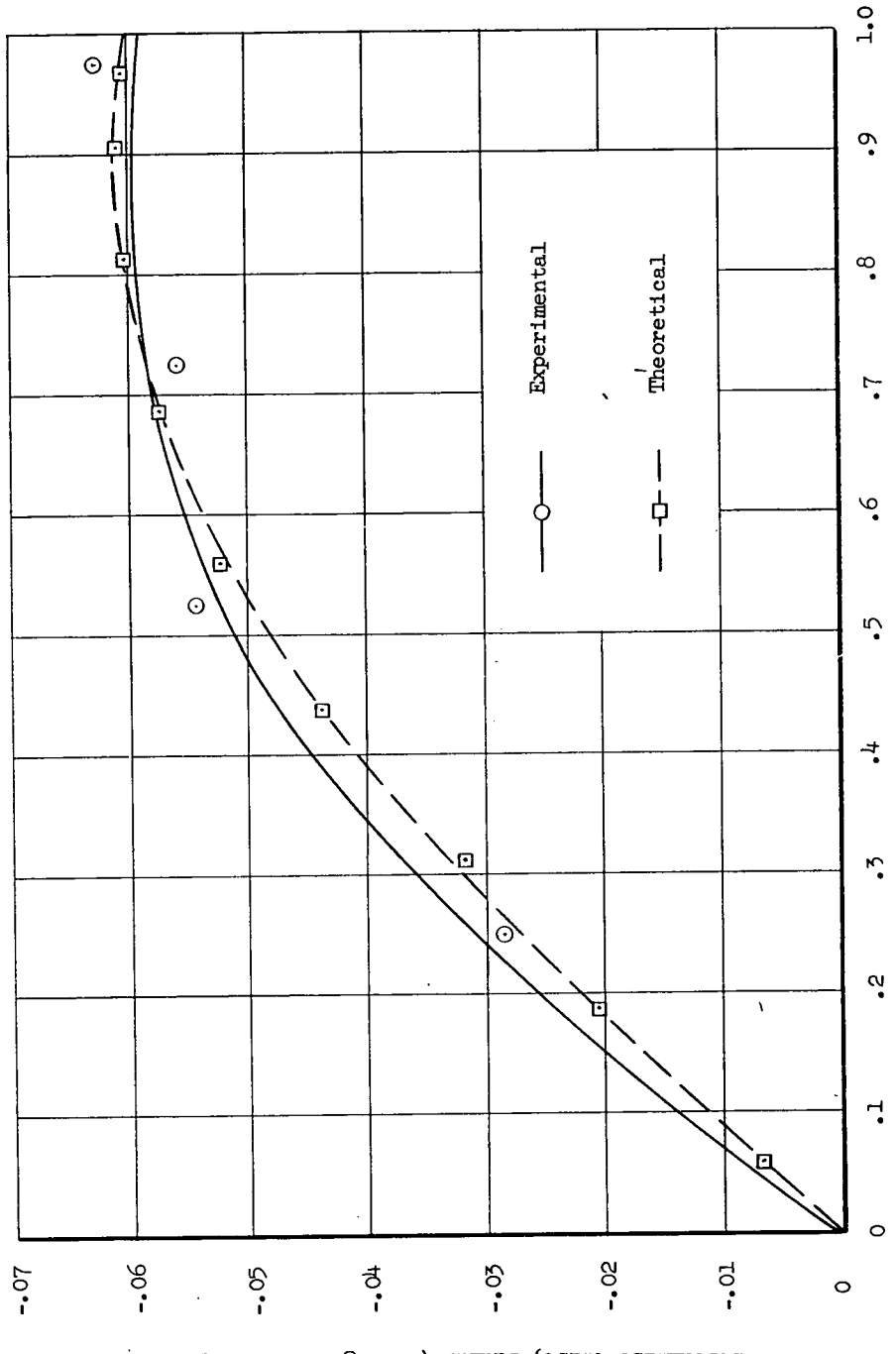

Figure 16.- Comparison of theoretical and experimental total streamwise twist. Altitude, 30,000 feet; Mach number, 0.66; airplane weight, 108,000 pounds; load factor, 2.2; $\dot{\theta}$ = 0.07 radian per second; $\dot{\theta}$ = -0.003 radian per second per second.

NACA-Langley - 4-14-55 - 350